Use of Lagrange polynomials to build refined theories for laminated beams, plates and shells

Use of Lagrage polinomials to build refined theories for laminated beams, plates and shells

A. Pagani [1]*, E. Carrera [1]†, R. Augello [1]‡, D. Scano [1]§

Mul[2] Group
[1]Department of Mechanical and Aerospace Engineering, Politecnico di Torino

Abstract: *This paper proposes an equivalent single-layer approach for modeling laminated structures, where the number layers to be considered as a single one is chosen a priori by the user. Lagrange points are set to locate and, eventually, join equivalent single-layer and layer-wise tenchiques by imposing displacement continuity in the thickness direction. The Finite Element (FE) method is applied to provide numerical solutions whereas the Carrera Unified Formulation (CUF) is used to generate the related stiffness matrices in a compact and straightforward way. The approach is employed using one-dimensional beam and two-dimensional plate and shell models and several case studies, taken from well-known examples in the literature, are analyzed. Results clearly show the advantages and superiority of the present approach to completely capture the displacements and the distribution of the axial stress components, whereas local values of the shear stresses can be obtained by opportunely chosing the Lagrange points pattern opportunely.*

Keywords: Composite structures; Equivalent Single Layer; Unified beam, plate and shell models.

1 Introduction

The constant development of sophisticated materials and components leads to increasingly complicated structural designs that require accurate and time-consuming analyses, in particular in the case of laminated composites. The difficulty of these analyses is mainly caused by the complex anisotropy of such structures, which may result into intricate mechanical phenomena. They are, for instance, the interlaminar continuity for the shear stresses and the zig-zag behaviour of the displacements (the C_z^0 requirements [1]), as well as the coupling between the in-plane and the out-of-plane strains. Nowadays, several theories and methods for the detailed analysis of laminated structures are available. An overview on the computational techniques for the analysis of one-dimensional (1D) laminated beams [2, 3] and two-dimensional (2D) plates, can be found in major review articles, see [2, 3] and [4, 5, 6], respectively. However, a brief discussion about some noteworthy contributions in the field is

*Full Professor. E-mail: alfonso.pagani@polito.it
†Full Professor. E-mail: erasmo.carrera@polito.it
‡Research Assistant. Corresponding author. E-mail: riccardo.augello@polito.it
§Post Graduate research Assistant. E-mail: daniele.scano@polito.it

given hereafter for the sake of completeness.
Classical theories such as the Euler-Bernoulli beam [7] is widely applied in numerical simulations, although it lacks the ability to accurately predict the transverse shear over the cross-section. To overcome this problem, many other models were developed to carry out reliable results, especially in the case of composite structures, see the Timoshenko beam theory [8], which considers a constant distribution of the shear stress along the cross-section.
Even though classical theories ensure reliable accuracy for a wide range of problems, they have some limitations. In fact, when dealing with thin-walled structures, whose cross-sectional deformation is relevant, an accurate evaluation of the stress distribution is necessary, to describe the higher-order phenomena. For this reason, advanced structural theories must be considered, because classical approaches might be inappropriate and lead to wrong conclusions. For instance, Stephen and Levinson [9] developed a higher-order theory starting from the Timoshenko beam equation and taking into account the shear curvature, through the introduction of new coefficients. As further examples of higher-order beam models proposed in the past, Vlasov [10] introduced warping functions to capture the deformations of beam cross-sections. This approach found a great success between scientists, see the works by Ambrosini *et al.* [11], Mechab *et al.* [12] and Friberg [13], who made use of warping functions for thin-walled structures. A combination of the refined Vlasov model and the classical Euler-Bernoulli model was adopted by Kim and Lee [14] to analyze thin-walled beams made of functionally graded materials. The so-called Generalized Beam Theory (GBT) was suggested by Schardt [15]. This theory allows the displacement field to be expressed as a linear combination of cross-sectional deformation modes. GBT found many applications in the literature, for example by Peres *et al.* [16] for the analysis of curved thin-walled beams, and by Silvestre [17] for buckling problems. GBT was also adopted for the analysis of laminated materials, as presented by Silvestre and Camotim [18, 19].
As far as the 2D plate and shell problerms are concerned, the former and probably the most famous 2D model is the classical Kirchhoff–Love theory [20, 21], whose extension to laminates is known as the Classical Lamination Theory (CLT) [22]. However, CLT neglects the effect of out-of-plane strains, and since one of the main issues related to the proper modelling of a composite structure is due to its low transverse shear moduli compared to the axial tensile moduli, CLT is therefore inadequate for most of the practical studies. On the other hand, the First Shear Deformation Theory (FSDT), which is based on the works by Reissner [23] and Mindlin [24], accounts for the shear deformation effects by linear variation of in-plane displacements. FSDT was widely developed in the framework of Finite Element Method (FEM) by Pryor and Barker [25], Noor [26], Hughes and Tezduyar [27] and many others and it still plays a fundamental role in commercial codes.
In order to overcome the limitations of classical theories, several refined plate Finite Elements (FEs) were developed over the last years. For instance, see the higher-order theories developed by Reddy [28], the so-called zig-zag theories [1], the theories based on the Reissner's Mixed Variational Theorem (RMVT) [6], and Layer-Wise (LW) models [29]. These higher-order theories assume refined expansion of the shear strains within the layers and were widely discussed by Kant et al. [30] and Kant and Kommineni [31]. Reddy [32] and Palazotto and Dennis [33] implemented higher-order theories fir plate and shell structures. Zig-zag theories, conversely, make use of piecewise zig-zag functions in the plate kinematics in order to fulfil the mechanical requirements demanded by composite laminates. Dozens of FEs were proposed based on zig-zag theories, see for example [34, 35, 36].
Most of the works discussed so far are based on an Equivalent Single Layer (ESL) approximation of the laminate. In ESL models, the variables are independent of the number of

layers. On the other hand, detailed analysis may require the adoption for Layer-Wise (LW) models, in which different sets of variables are considered per each layer. FE implementations of LW theories were proposed by many authors, such as for example Rammerstorfer et al. [37], Reddy [38], Mawenya and Davies [39], and Noor and Burton [40]. However, it has to be pointed out that the enhanced accuracy of LW models demands high computational costs. Thus, in the last years, several efforts were addressed by researchers to make the composite plate and shell models as accurate as efficient. A possible solution for tackling this problem is to combine multiple kinematics within the same mathematical model, in a global/local sense. In this manner, the computational costs can be reduced opportunely and the analysis enhanced only in those regions of the problem domain where higher accuracy is necessary. One of the simplest type of multiple-model method, for composite laminates analysis, is the concept of selective ply grouping or sublaminates [41, 42, 43]. This approach consists in creating some local regions along the plate/shell thickness, identified by specific ply or plies, within which accurate stresses are desired. On the other hand, in the global region, which is the domain portion where accurate analysis is not needed, lower-order and eventually ESL models can be adopted. Both ESL and LW models may eventually be implemented by using a combination of Lagrange and Legendre polynomials for formulating the theory kinematics along the thickness. In this manner, the primary variables between local and global regions can be immediately satisfied. In the work by Botshekanan Dehkordi et al. [44], a variable-kinematic description in the thickness direction for the static analysis of sandwich plates was performed. That model was derived in the framework of the Carrera Unified Formulation (CUF) and Reissner-Mixed-Variational-Theorem (RMVT) was adopted to describe a-priori the transverse shear and normal stresses. Thus, the transverse stresses were approximated through a mixed LW/ESL approach. The same mixed LW/ESL approach with RMVT was then used in Ref. [45] for nonlinear dynamic analysis of sandwich plates with flexible core and composite faces embedded with shape memory alloy wires. The global/local sublaminates approach was already exploited in the context of CUF for plates and shells (see [46, 47, 48]). In this work, it is applied on beam, plate and shell models, using Lagrange polynomials.
These models makes use of the variable-kinematic modelling features of CUF, which was developed by Carrera more than one decade ago [49, 50] and allows for the automatic and eventually hierarchical formulation of the theory of structures by using an extensive index notation and low- to higher-order generalized expansions of the primary mechanical variables. Thanks to CUF, both ESL and LW theories can be formulated with ease and eventually combined as in the case of the present variable kinematics beam, plate and shell elements.
The paper is organized as follows: Sections 2 and 3 describes beam, plate and shell theories and their FE models; Section 4 accurately describe the ESL model used in this paper; Section 5 reports the main numerical obtained results and, finally, the main conclusions are drawn.

2 Unified formulation of composite structures

Consider the composite laminates in Fig. 1. Albeit plate and shell structures are considered, both 1D and 2D mathematical models can be employed in principle.
For the 1D model, the cross-section Ω lays on the x, z-plane of a Cartesian reference system (x, y, z). As a consequence, the beam axis is placed along the y direction. The 2D plate and shell models uses the z coordinate for the thickness direction, and the latter uses a curvilinear reference frame (α, β, z) to account for the curvature, where α and β are the two in-plane directions. In this paper, single curvature shell structures are considered. The transposed

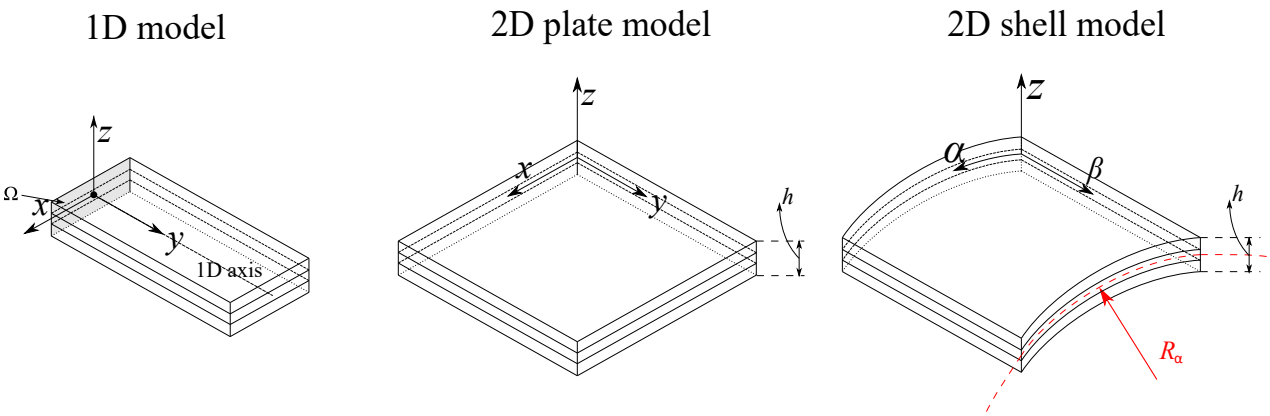

Figure 1: The modeling of generic composite structures using both 1D and 2D plate and shell models. For 1D model, y is the direction of the beam axis, whereas for the 2D models, z is the shell thickness coordinate. A Cartesian reference system is employed for the 1D beam and 2D plate model (x, y, z), whereas a curvilinear system (α, β, z) is used for the 2D shell model.

displacement vector for 1D beam and 2D plate models is introduced in the following:

$$\mathbf{u}(x,y,z) = \left\{ \begin{array}{ccc} u_x & u_y & u_z \end{array} \right\}^T \tag{1}$$

The stress, $\boldsymbol{\sigma}$, and strain, $\boldsymbol{\epsilon}$, components are expressed in vectorial form with no loss of generality,

$$\boldsymbol{\sigma} = \left\{ \begin{array}{cccccc} \sigma_{xx} & \sigma_{yy} & \sigma_{zz} & \sigma_{xz} & \sigma_{yz} & \sigma_{xy} \end{array} \right\}^T, \quad \boldsymbol{\epsilon} = \left\{ \begin{array}{cccccc} \epsilon_{xx} & \epsilon_{yy} & \epsilon_{zz} & \epsilon_{xz} & \epsilon_{yz} & \epsilon_{xy} \end{array} \right\}^T \tag{2}$$

As far as the 2D shell model is concerned, the three-dimensional (3D) displacement transposed vector $\mathbf{u}$ of a given point in the continuum shell is:

$$\mathbf{u}(\alpha,\beta,z) = \left\{ \begin{array}{ccc} u_\alpha & u_\beta & u_z \end{array} \right\}^{\mathrm{T}}, \tag{3}$$

The transposed strain ($\boldsymbol{\epsilon}$) and stress ($\boldsymbol{\sigma}$) vectors defined in the curvilinear reference system are:

$$\boldsymbol{\sigma} = \left\{ \begin{array}{cccccc} \sigma_{\alpha\alpha} & \sigma_{\beta\beta} & \sigma_{zz} & \sigma_{\alpha z} & \sigma_{\beta z} & \sigma_{\alpha\beta} \end{array} \right\}^{\mathrm{T}}, \quad \boldsymbol{\epsilon} = \left\{ \begin{array}{cccccc} \epsilon_{\alpha\alpha} & \epsilon_{\beta\beta} & \epsilon_{zz} & \epsilon_{\alpha z} & \epsilon_{\beta z} & \epsilon_{\alpha\beta} \end{array} \right\}^{\mathrm{T}}, \tag{4}$$

Regarding geometrical relations, they are expressed as

$$\boldsymbol{\epsilon} \ = \mathbf{b}\mathbf{u} \tag{5}$$

where $\mathbf{b}$ is the matrix of differential operators. It is different according to the employed mathematical model, and it reads:

$$\mathbf{b}_{\text{1D and 2D plate}} = \begin{bmatrix} \partial_x & 0 & 0 \\ 0 & \partial_y & 0 \\ 0 & 0 & \partial_z \\ \partial_z & 0 & \partial_x \\ 0 & \partial_z & \partial_y \\ \partial_y & \partial_x & 0 \end{bmatrix}, \qquad \mathbf{b}_{\text{2D shell}} = \begin{bmatrix} \frac{\partial_\alpha}{H_\alpha} & 0 & \frac{1}{H_\alpha R_\alpha} \\ 0 & \frac{\partial_\beta}{H_\beta} & \frac{1}{H_\beta R_\beta} \\ 0 & 0 & \partial_z \\ \partial_z - \frac{1}{H_\alpha R_\alpha} & 0 & \frac{\partial_\alpha}{H_\alpha} \\ 0 & \partial_z - \frac{1}{H_\beta R_\beta} & \frac{\partial_\beta}{H_\beta} \\ \frac{\partial_\beta}{H_\beta} & \frac{\partial_\alpha}{H_\alpha} & 0 \end{bmatrix}, \tag{6}$$

where $\partial_x = \dfrac{\partial(\cdot)}{\partial x}$, $\partial_y = \dfrac{\partial(\cdot)}{\partial y}$, $\partial_z = \dfrac{\partial(\cdot)}{\partial z}$, $\partial_\alpha = \dfrac{\partial(\cdot)}{\partial \alpha}$, $\partial_\beta = \dfrac{\partial(\cdot)}{\partial \beta}$, $H_\alpha = (1 + \dfrac{z}{R_\alpha})$, and $H_\beta = (1 + \dfrac{z}{R_\beta})$.

For the constitutive relation, linear elastic metallic structures are considered in this work. Consequently, the constitutive relation reads as:

$$\boldsymbol{\sigma} = \mathbf{C}\boldsymbol{\epsilon}, \tag{7}$$

where and $\mathbf{C}$ is the material elastic matrix, whose explicit form can be found in many reference texts, see [51, 52].

The 3D displacement field $\mathbf{u}(x, y, z)$ of the 1D beam and 2D plate and shell models, within the framework of the Carrera Unified Formulation (CUF), can be expressed as a general expansion of the primary unknowns as follows:

$$\begin{array}{rcll} \mathbf{u}_{\text{1D beam}}(x,y,z) & = & F_\tau(x,z)\mathbf{u}_\tau(y) & \\ \delta\mathbf{u}_{\text{1D beam}}(x,y,z) & = & F_s(x,z)\delta\mathbf{u}_s(y) & \\ & & & \\ \mathbf{u}_{\text{2D plate}}(x,y,z) & = & F_\tau(z)\mathbf{u}_\tau(x,y), & \tau = 1,2,....,M \\ \delta\mathbf{u}_{\text{2D plate}}(x,y,z) & = & F_s(z)\delta\mathbf{u}_s(x,y), & s = 1,2,....,M \\ & & & \\ \mathbf{u}_{\text{2D shell}}(\alpha,\beta,z) & = & F_\tau(z)\mathbf{u}_\tau(\alpha,\beta) & \\ \delta\mathbf{u}_{\text{2D shell}}(\alpha,\beta,z) & = & F_s(z)\delta\mathbf{u}_s(\alpha,\beta) & \end{array} \tag{8}$$

where F_τ and F_s are the expansion functions of the generalized displacements $\mathbf{u}_\tau$ and generalized virtual variations $\mathbf{u}_s$, the summing convention with the repeated indeces τ and s is assumed and M denotes the order of expansion. The choice of the expansion functions is a crucial topic for the present work, and are descibed hereafter.

2.1 Taylor-like expansions

It is clear that classical as well as higher-order theories can be easily obtained from Eq. (8) by using polynomials of different order as F_τ and F_s. This class of models was addressed as

to Taylor expansion models in the CUF literature [53] and they have proven good efficacy in the analysis of thin and homogeneous structures. For 1D case, the kinematics of the generic Taylor expansion model of order two is given in the following for the sake of completeness:

$$\begin{aligned} u_x(x,y,z) &= u_{x_1}(y) + u_{x_2}\, x + u_{x_3}\, z + u_{x_4}\, x^2 + u_{x_5}\, xz + u_{x_6}\, z^2 \\ u_y(x,y,z) &= u_{y_1}(y) + u_{y_2}\, x + u_{y_3}\, z + u_{y_4}\, x^2 + u_{y_5}\, xz + u_{y_6}\, z^2 \\ u_z(x,y,z) &= u_{z_1}(y) + u_{z_2}\, x + u_{z_3}\, z + u_{z_4}\, x^2 + u_{z_5}\, xz + u_{z_6}\, z^2 \end{aligned} \tag{9}$$

For 2D cases, it reads:

$$\begin{aligned} u_x(x,y,z) &= u_{x_1}(y) + u_{x_2}\, z + u_{x_3}\, z^2 \\ u_x(x,y,z) &= u_{y_1}(y) + u_{y_2}\, z + u_{y_3}\, z^2 \\ u_x(x,y,z) &= u_{z_1}(y) + u_{z_2}\, z + u_{z_3}\, z^2 \end{aligned} \tag{10}$$

2.2 Lagrange expansions

The cross-section is approximated with a pattern of Lagrange Points (LPs), which are divided into opportune Lagrange polynomials. The 3D displacement field is, then, a result of an interpolation of the displacements calculated at the LPs. The degree of the interpolation is defined by the number of the employed LPs. The number of DOFs equals the sum of the displacements for each LP. For instance, if a quadratic interpolation is empolyed, the interpolation functions for the 1D beam models are:

$$\begin{aligned} F_\tau &= \frac{1}{4}(r^2 + rr_\tau)(s^2 + ss_\tau) && \tau = 1,3,5,7 \\ F_\tau &= \frac{1}{2}s_\tau^2(s^2 - ss_\tau)(1-r^2) + \frac{1}{2}r_\tau^2(r^2 - rr_\tau)(1-s^2) && \tau = 2,4,6,8 \\ F_\tau &= (1-r^2)(1-s^2) && \tau = 9 \end{aligned} \tag{11}$$

where r and s are the natural coordinates from -1 to $+1$ of a generic point on the cross-section, and r_τ and s_τ are the natural coordinates of the nine LPs, as shown in Fig. 2(a). Readers are referred to [53] for the mathematical steps to transform the natural coordinates Eq. (11) into physical ones Eq. (8).

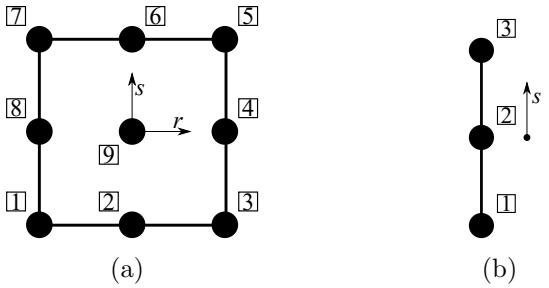

Figure 2: Example of a Lagrange element with 9 Lagrange points for beams (a) and a Lagrange element with 3 Lagrange points for plates and shells (b).

For the 2D plates and shells, the Lagrange polynomials for the quadratic interpolation are:

$$\begin{aligned} F_\tau &= \frac{1}{2}(s^2 + ss_\tau) && \tau = 1,3 \\ F_\tau &= -s^2 + 1 && \tau = 2 \end{aligned} \tag{12}$$

where s vary from -1 to $+1$, whereas s_τ correspond to the position of the LPs in the natural coordinate, as shown in Fig. 2(b) see [53] for more details.
It is clear that the expansion function describe a 2D cross-sectional domain for 1D beam models (see Fig. 3(a,b)), whereas a 1D thickness one for 2D plate and shell models (Fig. 3(c,d)).

3 Finite Element Approximation

The Finite Element Method (FEM) is adopted to discretize the generalized displacements $\mathbf{u}_\tau$ and the generalized variations $\mathbf{u}_s$. Thus, they are approximated as follows:

$$\begin{array}{lcll} \mathbf{u}_\tau(y) & = & N_i(y)\mathbf{q}_{\tau i} & \\ \delta\mathbf{u}_s(y) & = & N_j(y)\delta\mathbf{q}_{sj} & \\ & & & \\ \mathbf{u}_\tau(x,y) & = & N_i(x,y)\mathbf{q}_{\tau i}, & i = 1,2,....,N_n \\ \delta\mathbf{u}_s(x,y) & = & N_j(x,y)\delta\mathbf{q}_{sj}, & j = 1,2,....,N_n \\ & & & \\ \mathbf{u}_\tau(\alpha,\beta) & = & N_i(\alpha,\beta)\mathbf{q}_{\tau i} & \\ \delta\mathbf{u}_s(\alpha,\beta) & = & N_j(\alpha,\beta)\delta\mathbf{q}_{sj} & \end{array} \tag{13}$$

where N_i and N_j stands for the shape functions, the repeated subscripts i and j indicate summation, N_n is the number of the FE nodes per element and $\mathbf{q}_{\tau i}$ and $\mathbf{q}_{sj}$ are the following vectors of the FE nodal parameters:

$$\begin{array}{lcl} \mathbf{q}_{\tau i\ \text{1D and 2D plate}} & = & \left\{q_{x_\tau i}\ q_{y_\tau i}\ q_{z_\tau i}\right\}^T \\ \mathbf{q}_{sj\ \text{1D and 2D plate}} & = & \left\{q_{x_s j}\ q_{y_s j}\ q_{z_s j}\right\}^T \\ & & \\ \mathbf{q}_{\tau i\ \text{2D shell}} & = & \left\{q_{\alpha_\tau i}\ q_{\beta_\tau i}\ q_{z_\tau i}\right\}^T \\ \mathbf{q}_{sj\ \text{2D shell}} & = & \left\{q_{\alpha_s j}\ q_{\beta_s j}\ q_{z_s j}\right\}^T \end{array} \tag{14}$$

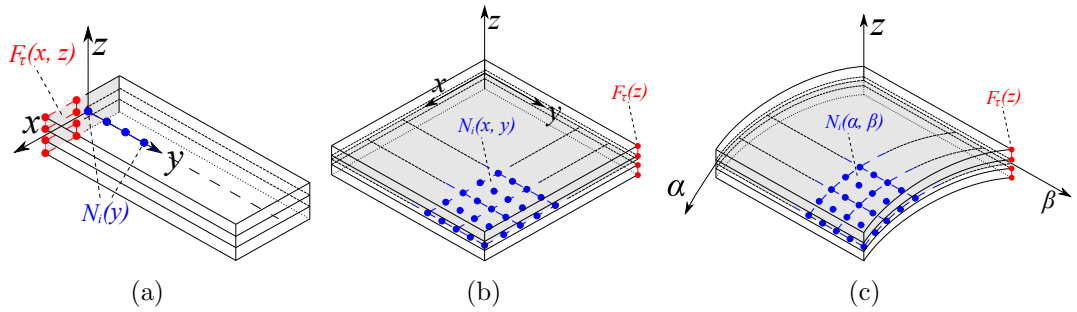

(a) (b) (c)

Figure 3: Mathematical models of the 1D beam (a, b), 2D plate (c) and shell (d) models of generic composite structures.

3.1 Governing equations

The principle of virtual displacements for a multi-layered plate structure reads:

$$\int_{\mathrm{V}} (\delta\boldsymbol{\epsilon}^T\boldsymbol{\sigma})\mathrm{dV} \quad = \quad \delta L_e \tag{15}$$

where V is the volume of the body. The left-hand side of the equation represents the variation of the internal work, while the right-hand side is the virtual variation of the external work. Substituting the geometrical relations (Eq. (5)), the constitutive equation (Eq. (7)) and applying CUF (Eq. (8)) and FEM (Eq. (13)), one obtains the following governing equations:

$$\delta \mathbf{q}_{sj}^{T} \, \mathbf{K}^{ij\tau s} \, \mathbf{q}_{\tau i} = \mathbf{P}_{sj} \tag{16}$$

where $\mathbf{K}^{ij\tau s}$ is a 3×3 matrix, called fundamental nucleus of the mechanical stiffness matrix. The nucleus is the basic element from which the stiffness matrix of the whole structure is computed. The fundamental nucleus is expanded on the indexes τ and s to obtain the stiffness matrix of each layer k. Then, the matrixes of each layer are assembled at the multi-layer level depending on the approach considered (see "Modelling approaches" section). $\mathbf{P}_{sj}$ is a 3×1 matrix, called fundamental nucleus of the external load. It explicit expression is not given here for the sake of brevity, but it can be found in [54] in the case of a point load.

4 Modelling approaches

Two different types of modelling approaches are usually adopted in the literature for the development of composite structure theories; i.e., ESL and LW. In this paper, CUF is employed for the formulation of a new approach for multilayered structure. This approach exploits the variable kinematics characteristics of CUF for the implementation of a structural element with mixed ESL/LW capabilities. Nevertheless, it is important to mention that the choice of the modelling approach (i.e., ESL, LW or variable kinematics) is independent of the type of the polynomials employed in the theory expansion within CUF.

4.1 ESL models

In an ESL model, the stiffness matrices of each layer are homogenized by simply summing the various contributions trough the thickness. This approach leads to a model that has a set of variables that is assumed for the whole multilayer, and thus is independent of the number of layers. In this work, ESL models that make use of both Taylor and Lagrange-like polynomials are used. For illustrative purposes, the general behaviour of the primary mechanical variables along the thickness of the structure in the case of ESL is depicted in Fig. 4(a).

4.2 LW models

In the case of LW, different sets of variables are assumed per each layer and the continuity of the displacements is imposed at the layer interface. The LW capability of describing correctly the discontinuous behaviour of the derivatives of the primary unknowns is graphically shown in Fig. 4(b). In this work, LW models are implemented by using Lagrange-like polynomial sets. In particular, the kinematic expansion is made by using Lagrange polynomials, see Eqs. (11) and (12). The compatibility condition is automatically ensured at each single LP.

4.3 Variable-kinematics

In this paper, a novel modelling approach for the analysis of multilayered structures is introduced. This method takes advantage of the variable kinematics feature of CUF formulation.

Thanks to CUF, in fact, different sets of F_τ and F_s functions can be employed to formulate advanced structural theories and opportunely tuned to obtain combined ESL/LW models for global/local analysis. In particular, in this work, ESL and LW approaches are combined by using structural theories based on Lagrange-like polynomials. In this variable-kinematics approach, multilayered structures can be modeled so as to have group of layers with homogenized properties as in a ESL assembling scheme, whereas for some other layers the homogenization is conducted just at the interface level to enforce LW capabilities in localized zones of the thickness domain.
The variable-kinematic assembling, developed in the framework of CUF, is very simple to be implemented with a few code statements. The coding lines of the terms of the nuclei, in fact, are the same for both ESL, LW and variable kinematic assembling. For the sake of completeness, the variable kinematic capability of the proposed methodology able to take into account non-local LW approach is shown in Fig. 4(c). Finally, an overview of the assembling procedures for ESL, LW and variable kinematics approaches is summarized in Fig. 5.

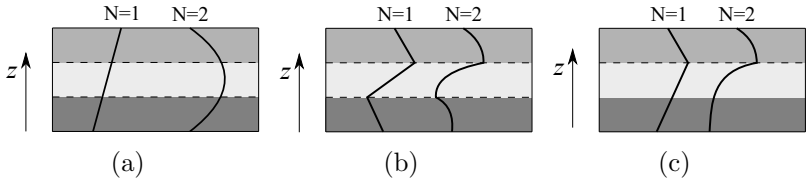

Figure 4: Equivalent-Single-Layer (a), Layer-Wise (b) and Variable-kinematics (c) behavior of the primary variables along the thickness.

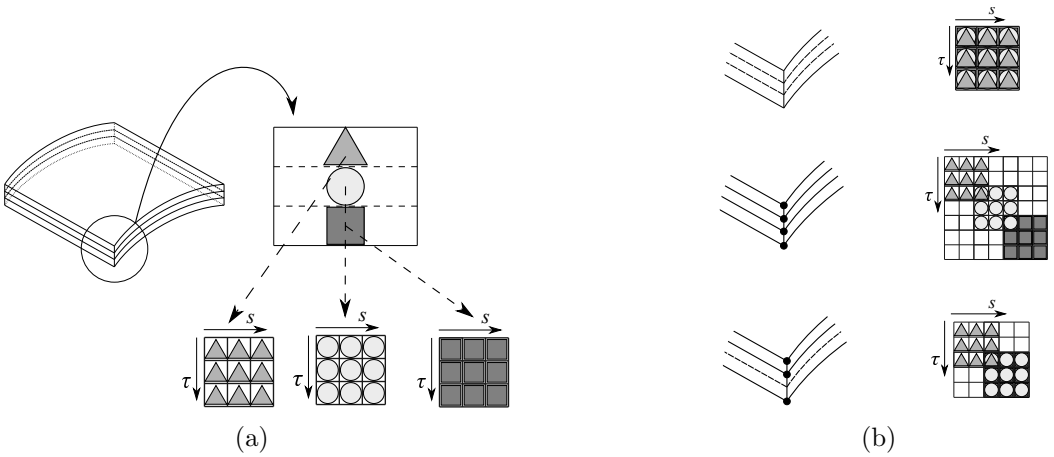

Figure 5: Assembling schemes of the 1D beam, 2D plate and shell models of generic composite structures.

5 Numerical results

Several analyses were conducted to prove the capability of the proposed ESL model to deal with beam, plate and shell structures. Whenever possible, 1D and 2D plate/shell models are used on the same study case. The LW models are recalled as "LN_{1D}" for 1D structures and "LN_{2D}" for 2D ones, respectively, where N stands for the order of the employed LPs (for

instance, "$L9_{1D}$" means that nine LPs are adopted for each layer of the beam structure and "$L4_{2D}$" means that four LPs are introduced for each layer of the plate/shell structure). On the other hand, ESL models are denoted with the letter "E" before the acronym, so that "$EL9_{1D}$" means that nine LPs are adopted using the ESL approach for a beam structure, and "$EL4_{2D}$" means that four LPs are used in an ESL framework for the plate/shell structure. Finally, "TBM" stands for Timoshenko Beam Theory, whereas "TEn_{1D}" and "TEn_{2D}" stand for the Taylor expansion of order n for 1D and 2D structures, respectively.

5.1 Eight-layer laminated structure

The first study deals with an eight-layer laminated structure. The analyzed case was taken from Ref. [55], along with the geometric and material properties. The structure was analyzed using 1D and 2D plate models. As far as the 1D models are concerned, the laminated structure was analyzed using both LW and ESL approaches. Three ESL approximations were adopted, using one (case A), two (case B) and four (case C) equispaced elements over the cross-sectional domain. Preliminary convergence analyses were conducted, and the results are shown in Fig. 6. Both LW (Fig. 6(a)) and ESL (Fig. 6(b)) techniques were investigated. The case with one element over the cross-section is employed for the ESL convergence study. The results show a faster convergence using B4 FEs. Thus, 10 B4 FEs are adopted for every following analysis. Static analyses are performed, with the structure being loaded with a transverse

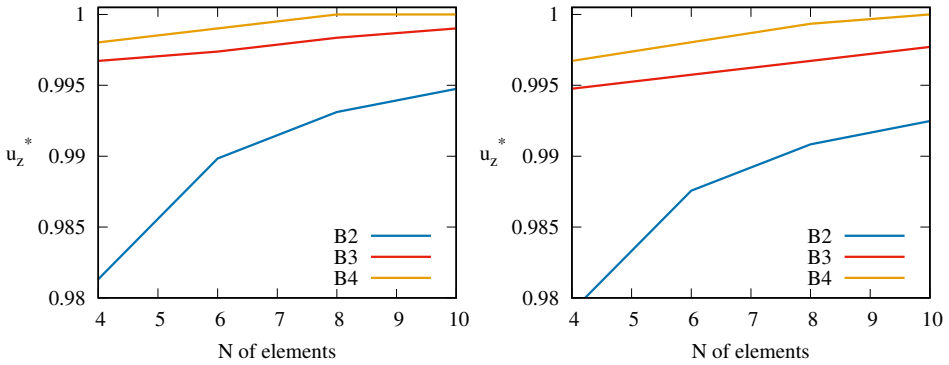

Figure 6: Convergence analyses of the eigth-layers laminated structure using LP with 1D LW (a) and ESL (b) approaches.

force equal to 0.05 N. Numerical results from several theories are reported in Table 1. Clearly, higher-oder models are close to the reference results, both in terms of displacement and axial stress. The distribution of the through-the-thickness axial and shear stress components are reported in Fig. 7. σ_{yy} distribution is accurately described by every theory, whereas the ESL models fail on adequately describe the local interlaminar σ_{yz} value.

Model	$-u_z \times 10^2 mm$ $[0, L, h/2]$	$\sigma_{yy} \times 10^3 MPa$ $[t/2, L/2, h/2]$	DOF
Ref.	3.031	730	—
TBM	2.988	730	155
$TE9_{1D}$	3.054	730	5115
$L16_{1D}$	3.050	730	9300
Case A			
$EL16_{1D}$	3.056	730	1488
Case B			
$EL16_{1D}$	3.056	730	2604
Case C			
$EL16_{1D}$	3.054	730	4836

Table 1: Transverse displacement and axial stress of the eigth-layers laminated structure using different 1D mathematical models. Ref. comes from [55]. One cross-sectional element for the "Case A", two and four equispaced elements for the "Case B" and "Case C", respectively.

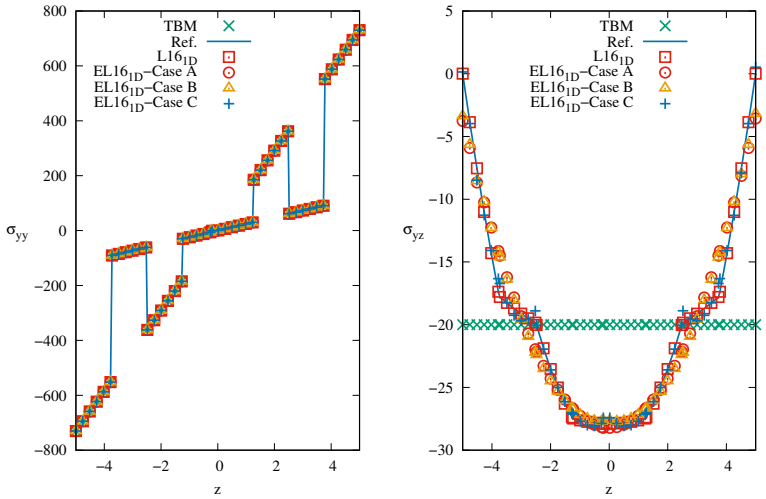

(a) (b)

Figure 7: Axial (a) and shear (b) stress distributions using different 1D mathematical models for the eigth-layers laminated structure. Ref. comes from [55]. One cross-sectional element for the "Case A", two and four equispaced elements for the "Case B" and "Case C", respectively.

Regarding the 2D analyses, three ESL approximations were adopted, using one, two and four equispaced elements over the thickness direction. Preliminary convergence analyses were carried out. The results are shown in Fig. 8 for both LW and ESL approaches, and, for the ESL approach, the one element case was considered. 10 Q9 elements resulted to be a reliable approximation and was adopted for every subsequent analyses. Then, the static analysis was performed using the converged FE approximation and different theories for the thickness expansion functions, and the numerical results are reported in Table 2. As in the 1D case, higher-order theories are needed to accurately evaluate the transverse displacement. Moreover, the axial and shear distrubutions are reported in Fig 9. The drawn conclusions are the same as in the previous 1D study, so that ESL models are able to accurately describe the σ_{yy} distribution, while failing for the σ_{yz}, in particular for the interlaminar description. If one puts LPs at the interlaminar level, the results are closer to the LW description of the problem. For instance, Fig. 9(c) reports the evaluation fo the first and second layer, and results perfectly match with the LW approach with the LPs at the interlaminar level, as also

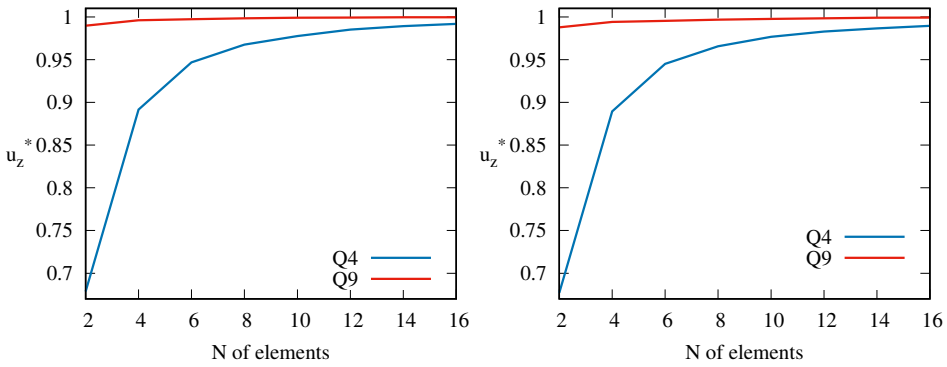

Figure 8: Convergence analyses of the eigth-layers laminated structure using LP with 2D LW (a) and ESL (b) approaches.

Model	$-u_z \times 10^2 mm$ $[0, L, h/2]$	$\sigma_{yy} \times 10^3 MPa$ $[b/2, L/2, h/2]$	DOF
Ref.	3.031	730	—
Reissner-Mindlin	2.988	732	495
$TE9_{2D}$	3.049	729	2970
$L4_{2D}$	3.050	729	7425
Case A			
$EL4_{2D}$	3.054	729	1188
Case B			
$EL4_{2D}$	3.054	729	2079
Case C			
$EL4_{2D}$	3.053	729	3861

Table 2: Transverse displacement and axial stress of the eigth-layers laminated structure using different 2D mathematical models. Ref. comes from [55]. One over-the-thickness element for the "Case A", two and four equispaced elements for the "Case B" and "Case C", respectively.

reported in Table 3.

Model	$\sigma_{yz} \times 10^3 MPa$ $[b/2, L/2, 3h/8]$	DOF
$TE9_{2D}$	-16.41	2970
$L4_{2D}$	-17.93	7425
$EL4_{2D}$-one layer	-17.93	2970
$EL4_{2D}$-two layers	-15.52	2970

Table 3: Interlaminar shear stress distributions using different 1D mathematical models for the eigth-layers laminated structure. "$EL4_{2D}$-one layer" consists in a LW description only for the first layer and the "$EL4_{2D}$-two layers" for the first two layers.

5.2 Simply supported plate with transverse force

The second analysis case regards a simply supported plate subjected to a transverse force, as shown in Fig. 10. The surface of the plate is a square and the thickness-to-side ratio a/h equals 100. The plate is made of 3 layers with $[0°/90°/0°]$ stacking sequence with the

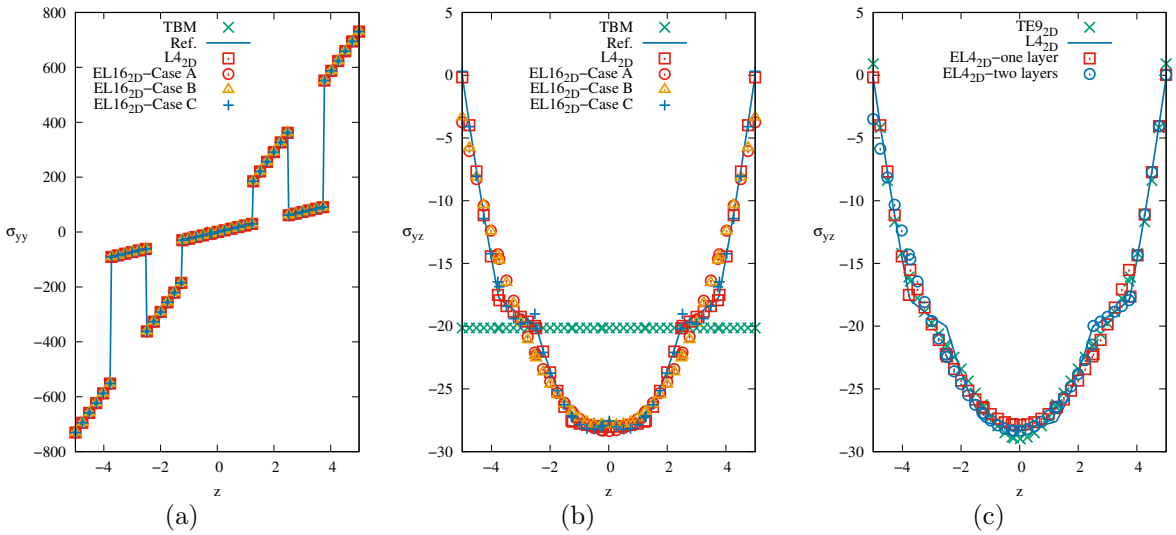

Figure 9: Cross-sectional discretization and LP pattern for different 2D ESL approaches. Ref. comes from [55]. One over-the-thickness element for the "Case A", two and four equispaced elements for the "Case B" and "Case C", respectively. "EL4$_{2D}$-one layer" consists in a LW description only for the first layer and the "EL4$_{2D}$-two layers" for the first two layers.

following material properties, $E_L/E_T = 25$, E_L=E_z, $\nu_{LT} = \nu_{Ta} = \nu_{La} = 0.25$ $G_{LT} = G_{Ta} = G_{La} = E_T$. The study case is taken from [56]. The adopted discretization approximations

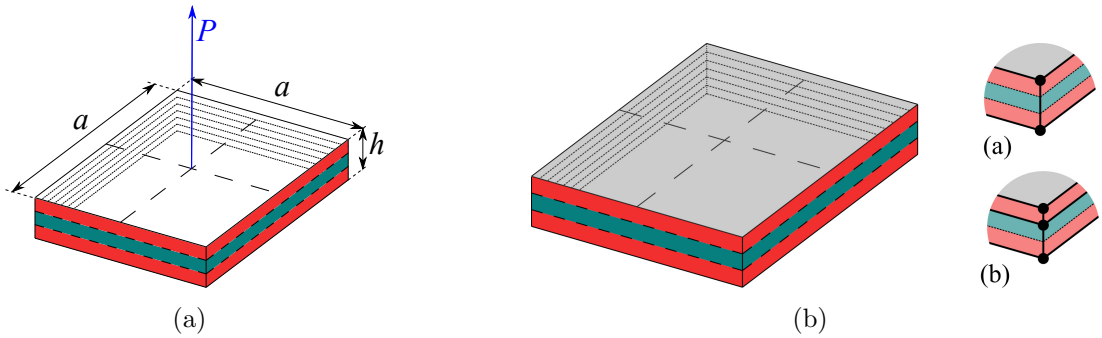

Figure 10: Geometric properties and loading case of the simply supported plate with transverse force (a). Discretizations and LP patterns for different 1D and 2D ESL approaches (b). 1 element (a) and 2 elements (b).

for both 1D and 2D ESL models are described in Fig. 10(b) and they involve 1 and 2 elements over the thickness. The LW discretization is used as well. Preliminary convergence analysis were conducted using 1D models. The results are reported in Fig. 11 and 6 B4 FEs are employed for all subsequent analyses. Then, static analyses were carried out using the converged FE model and adopting several theories. The results show a great difference between the obtained solutions and the reference results. The accuracy is improved if proper ESL model is employed, see the Fig. 10(b-a) kinematic model. The distributions are shown in Fig. 12, whereas correspondent values are reported in Table 4. Clearly, not even a refined 1D LW model can accurately describe the static behavior of the structure. This is due to the geometry of the structure, and a more refined model should be mandatory for the correct evaluation of the shear stress. The same analysis was conducted using 2D models. The convergence analyses are reported in Fig. 13, and 150 Q9 elements are adopted for the

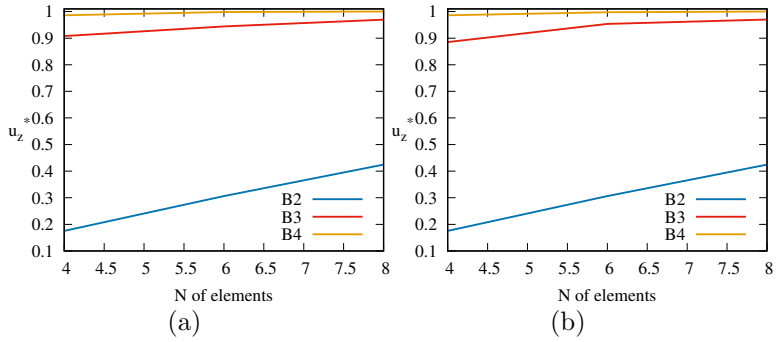

Figure 11: Convergence analyses of the simply supported plate using LP with 1D LW (a) and ESL (b) approaches. $u_z^* = \dfrac{u_z \times 100 E_2 h^3}{P a^3}$.

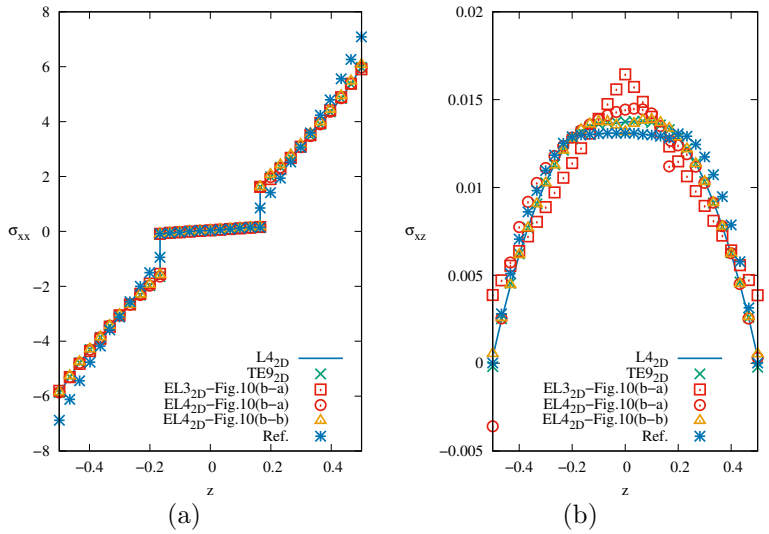

Figure 12: In-plane (a) and shear (b) stress distributions using different 1D mathematical models for the simply supported plate. Ref. comes from [56].

Model	$\overline{U}_z$ in $[a/2, b/2, 0]$	$\overline{\sigma}_{xx}$ in $[a/2, b/2, h/2]$	$\overline{\sigma}_{xz}$ in $[0, b/2, 0]$	DOF
Ref.	2.168	7.096	0.0131	—
$L16_{1D}$	2.189	6.264	0.0111	24375
$L9_{1D}$	2.185	5.663	0.0145	11475
$EL9_{1D}$-10(b-a)	2.185	5.633	0.0176	9375
$EL16_{1D}$-10(b-a)	2.189	6.262	0.0108	13125
$EL16_{1D}$-10(b-b)	2.221	6.371	0.0176	13125

Table 4: Transverse displacement, in-plane and shear stress of the simply supported plate using different 1D mathematical models. Ref. comes from [56]. Ref. comes from [56]. $\overline{U}_z = \dfrac{\overline{U}_z \times 100 E_2 h^3}{P a^3}$, $\overline{\sigma}_{xx} = \dfrac{\sigma_{xx}}{P}$ and $\overline{\sigma}_{xz} = \dfrac{\sigma_{xz}}{P}$.

subsequent analyses. The converged model is adopted for the static analysis. The in-plane and shear stress distributions are reported in Fig. 14. On the contrary of what arised from 1D modeling, a refined LW model leads to accurate results compared to the reference ones,

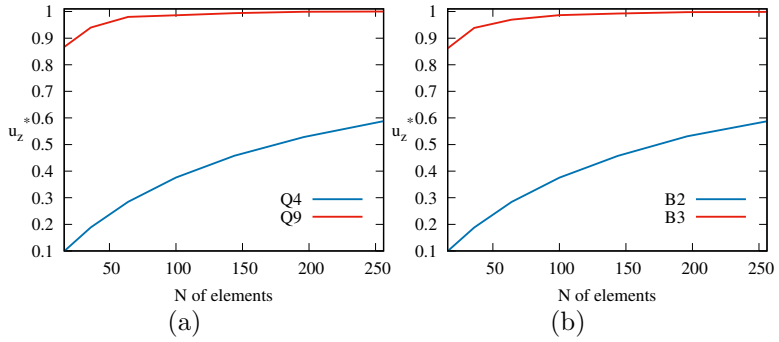

Figure 13: Convergence analyses of the simply supported plate using LP with 2D LW (a) and ESL (b) approaches.

both in terms of axial and shear stress. Correspondent value are reported in Table. 5.

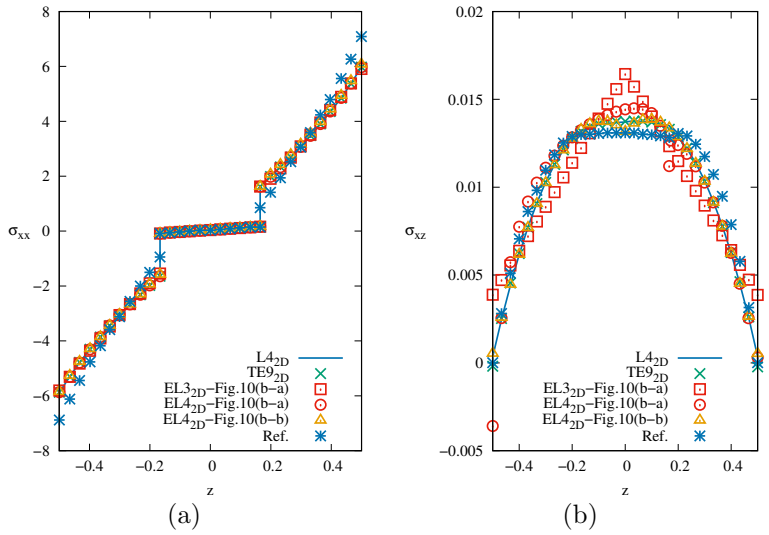

Figure 14: In-plane (a) and shear (b) stress distributions using different 1D mathematical models for the simply supported plate. Ref. comes from [56].

Model	$\overline{U}_z$ in $[a/2, b/2, 0]$	$\overline{\sigma}_{xx}$ in $[a/2, b/2, h/2]$	$\overline{\sigma}_{xz}$ in $[0, b/2, 0]$	DOF
Ref.	2.168	7.096	0.0131	—
$L4_{2D}$	2.175	5.976	0.0137	32799
$TE9_{2D}$	2.175	5.975	0.0137	25320
$EL4_{2D}$-10(b-a)	2.175	5.971	0.0131	17661
$EL4_{2D}$-10(b-b)	2.202	6.077	0.0144	17661

Table 5: Transverse displacement, in-plane and shear stress of the simply supported plate using different 2D mathematical models. Ref. comes from [56]. Ref. comes from [56]. $\overline{U}_z = \dfrac{\overline{U}_z \times 100 E_2 h^3}{P a^3}$, $\overline{\sigma}_{xx} = \dfrac{\sigma_{xx}}{P}$ and $\overline{\sigma}_{xz} = \dfrac{\sigma_{xz}}{P}$.

Finally, a comparison from the most accurate 1D and 2D results are shown in the same figure for comparison purposes, and the stress distribution and values are reported in Fig. 15 and Table 6.

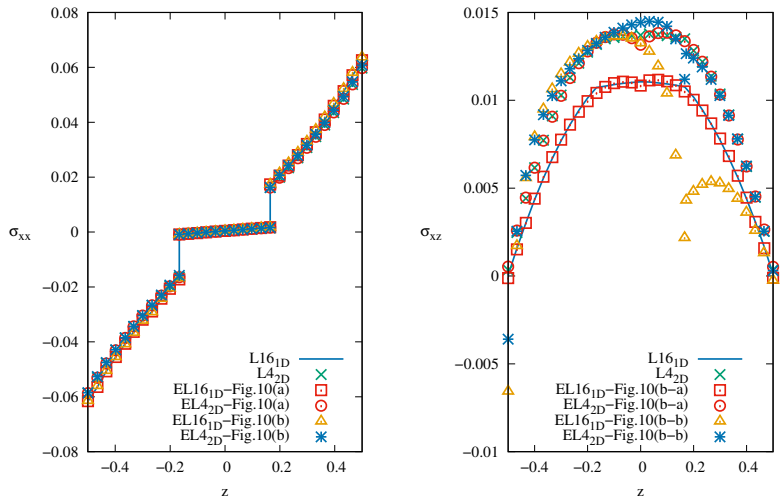

(a) (b)

Figure 15: In-plane (a) and shear (b) stress distributions using different 1D and 2D mathematical models for the simply supported plate.

Model	$\overline{U}_z$ in $[a/2, b/2, 0]$	$\overline{\sigma}_{xx}$ in $[a/2, b/2, h/2]$	$\overline{\sigma}_{xz}$ in $[0, b/2, 0]$	DOF
L16$_{1D}$	2.189	6.264	0.0111	24375
L4$_{2D}$	2.175	5.976	0.0137	32799
EL16$_{1D}$-10(b-a)	2.189	6.262	0.0108	13125
EL4$_{2D}$-10(b-a)	2.175	5.971	0.0131	17661
EL16$_{1D}$-10(b-b)	2.221	6.371	0.0176	13125
EL4$_{2D}$-10(b-b)	2.202	6.077	0.0144	17661

Table 6: Transverse displacement and axial stress of the simply supported plate using different 1D and 2D mathematical models. $\overline{U}_z = \dfrac{\overline{U}_z \times 100 E_2 h^3}{P a^3}$, $\overline{\sigma}_{xx} = \dfrac{\sigma_{xx}}{P}$ and $\overline{\sigma}_{xz} = \dfrac{\sigma_{xz}}{P}$.

5.3 Nine-layers plate

The capabilities of the present model to deal with composite structures is further proved with a nine-layers plate. The geometric and loading conditions are described in Fig. 16, where the surface of the plate is a square with side a, and $a/h = 10$. The stacking sequence is $[90°/0°/90°/0°/90°/0°/90°/0°/90°]$, and the plate is simply supported. The material properties are $E_L = 172$ GPa, $E_z = E_T = 6.9$ GPa, $\nu_{LT} = \nu_{zL} = \nu_{Tz} = 0.25$, $G_{LT} = 3.4$ GPa, $G_{zL} = G_{Tz} = 1.4$ GPa, where L stands for the longitudinal direction, and T for the transverse one. Finally, the plate is loaded with a tranverse bi-sinusoidal pressure $p = P_z \sin(\frac{\pi}{a}x)\sin(\frac{\pi}{a}y)$, with $P_z = 1$. This study case is taken from [57]. For this analysis, a 2D plate model is employed and preliminary convergence analyses are conducted. The results are reported in Figs. 17, for displacement and shear stress σ_{xz}. Both LW and ESL approaches are employed, using L4$_{2D}$ polynomials. Clearly, Q9 show a faster convergence than Q4, for both displacement and stress cases. Moreover, 100 Q9 FEs represents a reliable approximation, and, then, is used as converged mathematical model for the subsequent analyses. On the converged FE approximation, several through-the-thickness ESL discretizations are employed and they are reported in Fig. 16(b). They differ from the number of LPs and, consequently, elements adopted, so that Fig. 16(b-a) describes LPS on the thickness edges and this is the same approximation used

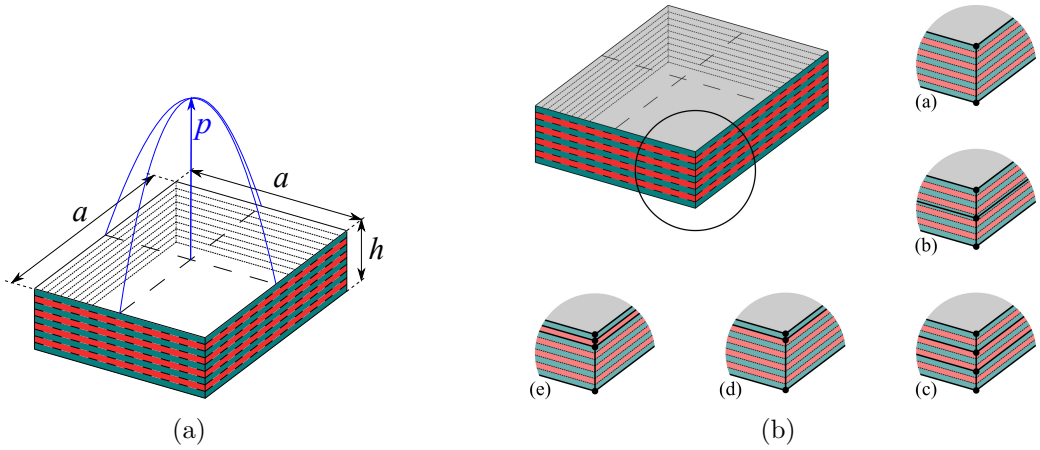

Figure 16: Geometric properties and loading case of the nine-layers plate with bi-sinusoidal pressure (a). Discretizations and LP patterns for different 2D ESL approaches (b). 1 element (b-a), 2 elements (b-b, b-d) and 3 elements (b-c, b-e).

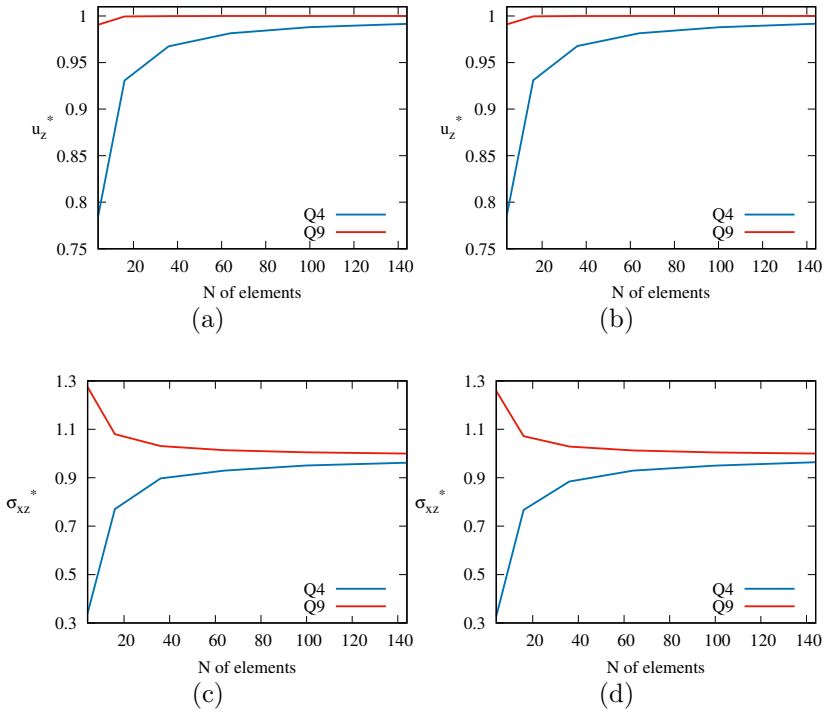

Figure 17: Displacement (a) and stress (b) convergence analyses and of the nine-layers plate using LP with 2D LW (a) and ESL (b) approaches. $u_z^* = \dfrac{u_z - u_{z_{140Q9}}}{u_{z_{140Q9}}}$, $\sigma_{xz}^* = \dfrac{\sigma_{xz} - \sigma_{xz_{140Q9}}}{\sigma_{xz_{140Q9}}}$.

for the convergence analysis. Figures 16(b-b) and 16(b-c) makes use of 2 and 3 elements along the thickness, whereas Figs. 16(b-d) and 16(b-e) focusses on the kinematic description of the first layer, using 2 and 3 elements, respectively. The described ESl mathematical models, along with LW and TE one, are adopted for the evaluation of axial and shear stress. Figure 18 reports the $\overline{\sigma}_{xx}$ distribution. Figure 18(a) reports the results of LW and TE models compared to the reference one ([57]). The results prove a great accuracy between the models, and the same agreement is highlighted in Fig. 18(b) using the ESL mathematical models of Fig.

16(b). Figure 19 reports the distribution of $\overline{\sigma}_{xz}$. A sligth difference between the ESL solutions

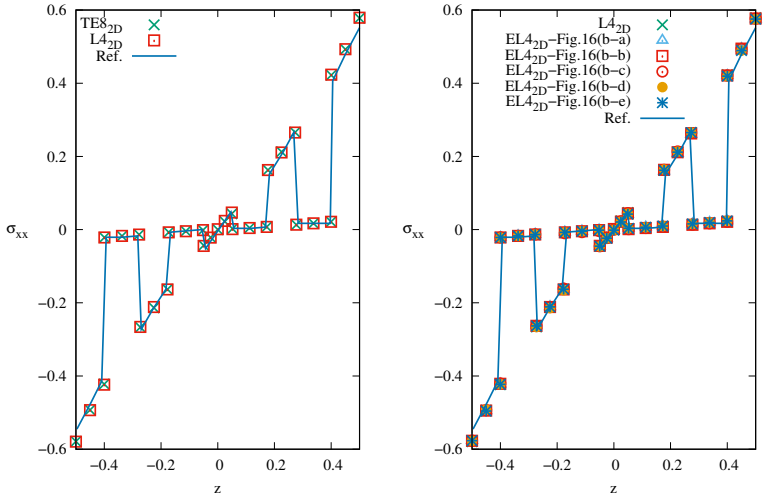

Figure 18: In-plane stress distributions using different 2D mathematical models for the nine-layers plate. Ref. comes from [57]. $\overline{\sigma}_{xx} = \dfrac{\sigma_{xx}h^2}{P_z a^2}$.

and the reference one is shown. Numerical values of $\overline{w}$, $\overline{\sigma}_{xz}$, $\overline{\sigma}_{xx}$ and $\overline{\sigma}_{yz}$ are evaluated, where $\overline{w}_z = \dfrac{\pi^4 U Q h^4}{12 P a^4}$, $\overline{\sigma}_{xx} = \dfrac{\sigma_{xx}h^2}{Pa^2}$, $\overline{\sigma}_{xz} = \dfrac{\sigma_{xz}h}{Pa}$, $\overline{\sigma}_{yz} = \dfrac{\sigma_{yz}h}{Pa}$, and $Q = 4G_{12} + \dfrac{[E_1 + E_2(1+2\nu_{12})]}{1-\nu_{12}\nu_{31}}$. However, if one is interested on a specific value of the shear stress, an opportune pattern of LPs can be included in the model. For instance, Table 7 reports the numerical values of $\overline{\sigma}_{xz}$ using the ESL mathematical models reported in Figs. 16(b-d) and 16(b-e). Clearly, The EL4-16(b-e) can accurately evaluate the stress value, compared to the L4$_{2D}$ model, with the 35% of the DOFs. Finally, the distribution of the first two layers is reported in 19(c) and

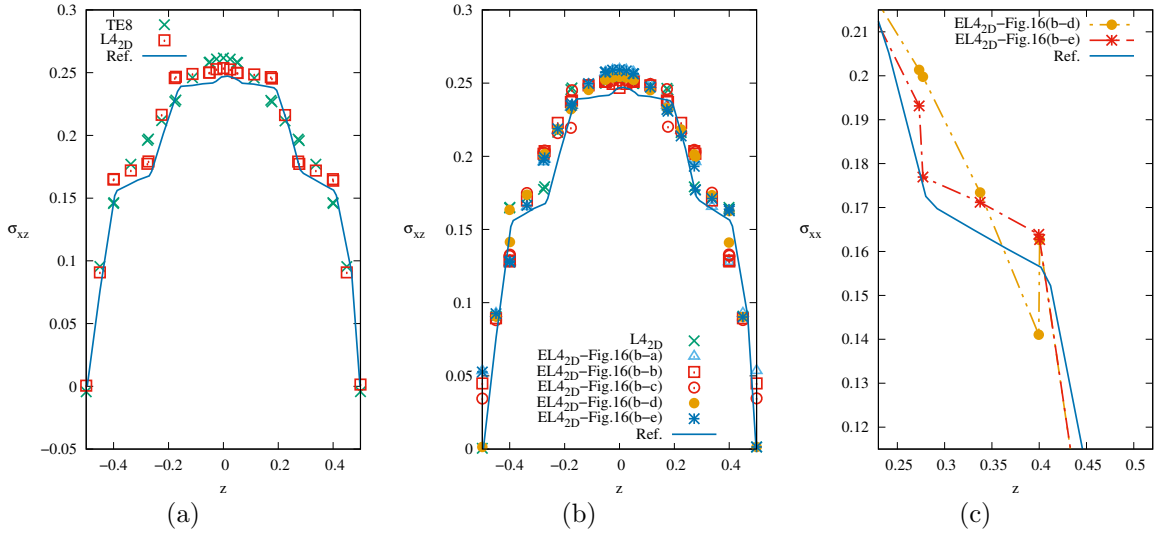

Figure 19: Shear stress distributions using different 2D mathematical models for the nine-layers plate. Ref. comes from [57]. $\overline{\sigma}_{xz} = \dfrac{\sigma_{xz}h}{P_z a}$.

Model	$\overline{w}$ $(a/2, a/2, 0)$	$\overline{\sigma}_{xz}$ $(0, a/2, 0)$	$\overline{\sigma}_{xx}$ $(a/2, a/2, h/2)$	$\overline{\sigma}_{yz}$ $(a/2, 0, 0)$	DOF
Ref.	1.512	0.247	0.551	0.226	—
$L4_{2D}$	1.5356	0.2536	0.5792	0.2304	37044
$TE8_{2D}$	1.5335	0.2617	0.5779	0.2217	11907
Fig.16(b-a)					
$EL4_{2D}$	1.5234	0.2593	0.5755	0.2299	5292
Fig.16(b-b)					
$EL4_{2D}$	1.5315	0.2467	0.5768	0.2312	9261
Fig.16(b-c)					
$EL4_{2D}$	1.5315	0.2518	0.5770	0.2330	13230
Fig.16(b-d)					
$EL4_{2D}$	1.5284	0.2542	0.5751	0.2331	13230
Fig.16(b-e)					
$EL4_{2D}$	1.5278	0.2592	0.5753	0.2296	13230

Table 7: Transverse displacement, in-plane and shear stress of the nine-layers plate using different 2D mathematical models. Ref. comes from [56]. $\overline{w}_z = \dfrac{\pi^4 U Q h^4}{12 P a^4}$, $\overline{\sigma}_{ii} = \dfrac{\sigma_{ii} h^2}{P a^2}$, $\overline{\sigma}_{ij} = \dfrac{\sigma_{ij} h}{P a}$, where $Q = 4G_{12} + \dfrac{[E_1 + E_2(1 + 2\nu_{12})]}{1 - \nu_{12}\nu_{31}}$. Ref. comes from [57].

Table 8.

Model	$\overline{\sigma}_{xz}$ $[0, a/2, 2h/5]$	DOF
$TE8_{2D}$	0.1464	11907
$L4_{2D}$	0.1651	37044
$EL4_{2D}$-Fig.16(b-d)	0.1410	13230
$EL4_{2D}$-Fig.16(b-e)	0.1639	13230

Table 8: Interlaminar shear stress distributions using particular 2D mathematical models for the nine-layers plate. $\overline{\sigma}_{xz} = \dfrac{\sigma_{xz} h}{P a}$.

5.4 Cylindrical shell subjected to pressure

Finally, a study case of a cylindrical shell subjected to transverse pressure is reported here. The analysis was originally proposed by Ren [58] and further investigated by Carrera [50]. The geometric properties and loading conditions are reported in Fig. 20. A curvilinear reference system is adopted, and the shell curvature is on the β axis. The material properties are $E_L/E_T = 25$, $G_{LT}/E_T = 0.5$, $G_{TT}/E_T = 0.2$, $\nu_{LT}/\nu_{TT} = 0.25$, $R_\beta/b = \pi/3$, $R_\beta/h = 4$ and $a = 10$. The longitudinal direction lays on the α axis and the stacking sequence is $[90°/0°/90°]$. The shell is simply supported on its longitudinal edges. Preliminary convergence analyses were carried out for the evaluation of the FE mesh. The results are reported in Fig. 21, and 24 Q9 FEs is demonstrated to be a reliable approzimation for both LW (Fig. 21(a, c)) and ESL (Fig. 21(b, d)) cases. A static analysis is performed. The LW and ESL models are used, and the results are compared to those available. The ESL discretizations are reported in Fig. 22 (a, b, c) and, in the same figure, the distrubutions of the through-the-thickness shear stress is reported. A general good agreement of the LW approach is clear, whereas the ESL models fails on describing the overall distribution. Nevertheless, if a single layer is interested, one

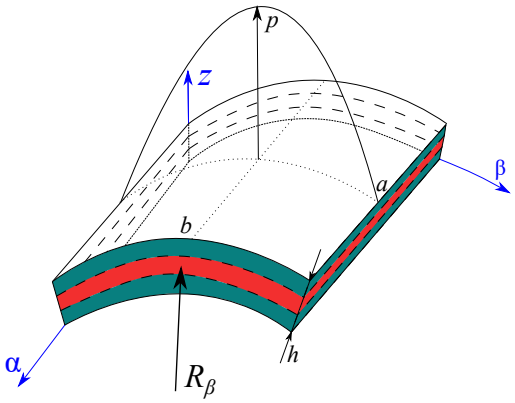

Figure 20: Geometric properties and loading case of the shell subjected to pressure.

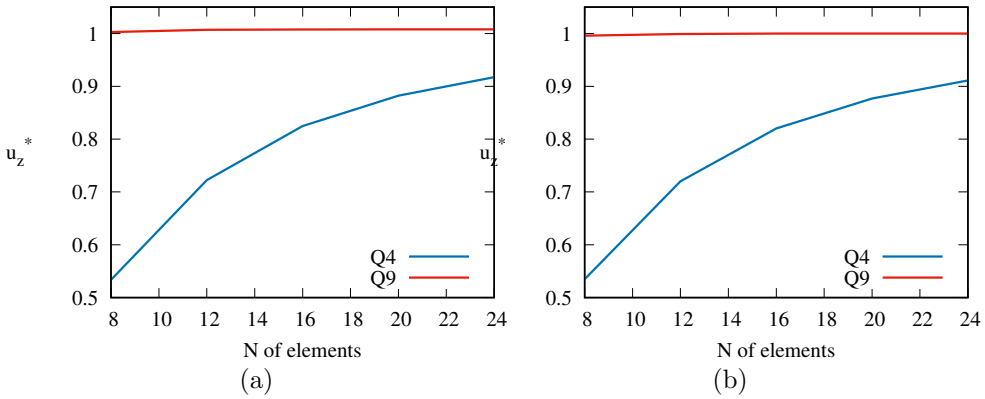

Figure 21: Convergence analyses of the cylindrical shell subjected to pressure using LP with 2D LW (a) and ESL (b) approaches. $u_z^* = \dfrac{u_z^* \times 10E_2h^3}{PR_\beta^4}$.

can put LPs oppourtunely to descrive the behavior, as for the mathematical model described in Fig. 22 (c). Finally, the numerical values are reportd in Table 9.

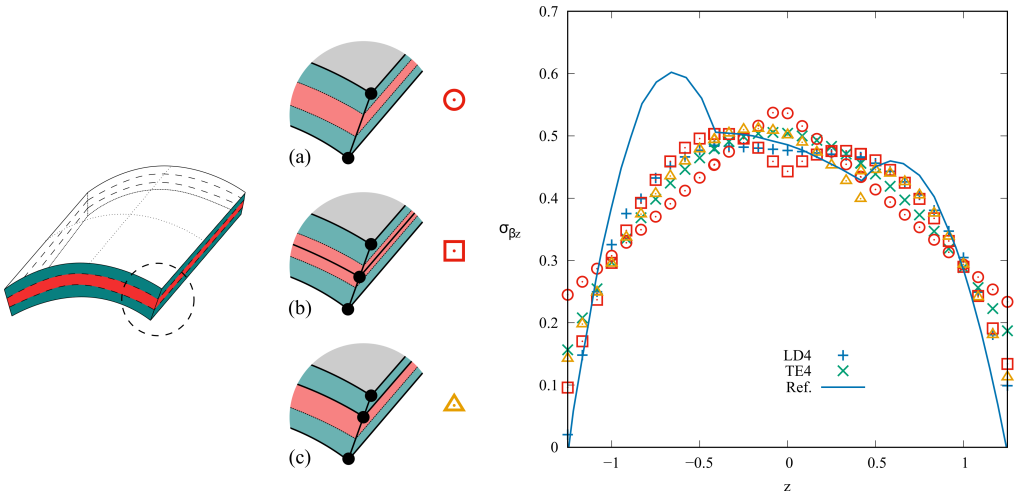

Figure 22: Shear stress distributions using different 2D mathematical models for the cylindrical shell subjected to pressure. $\overline{\sigma}_{\beta z} = \dfrac{\sigma_{\beta z}h}{PR_\beta}$. Ref. comes from [50].

Model	$\overline{U}_z$ in $[b/2, a/2, 0]$	$\overline{\sigma}_{\beta z}$ in $[0, b/2, 0]$	DOF
Ref.(1)	0.4570	0.476	—
Ref.(2)	0.4593	0.487	—
$L4_{2D}$	0.4596	0.485	14763
Fig.22(a)			
$EL3_{2D}$	0.3281	0.572	3108
Fig.22(b)			
$EL4_{2D}$	0.3834	0.405	5439
Fig.22(c)			
$EL4_{2D}$	0.4501	0.501	2625

Table 9: Transverse displacement, in-plane and shear stress of the cylindrical shell subjected to pressure using different 2D mathematical models. Ref.(1) comes from [58]. Ref.(2) comes from [50].

6 Conclusions

The present research work was addressed to evaluate the performances and benefits of adopting an Equivalent Single-Layer (ESL) approach based on the Lagrange polynomials in the static analysis of composite beams, plates and shells. Various geometries were analyzed and one-dimensional (1D) beams and two-dimensional (2D) plate and shell models were compared each other, whenever possible. Point loadings and sinusoidal pressures were considered. Each case study was taken from well-known literature problems, so that numerical results are compared with the analytical ones.
Results show the advantage of adopting ESL based on the Lagrange polynomials in the proposed cases. The following main conclusions can be summarized:

- The proposed ESL approach is a powerful method to reduce computational cost in static problems, and this is confirmed clearly by the various case studies reported in this paper;
- Higher/lower order kinematics can be introduced easily in the regions of the structures which show higher/lower local phenomena.;
- No drawbacks or numerical issues were found;
- The mixing of various through-the-thickness kinematics between two adjacent layers is done simply by imposing continuity at Lagrange points, so that no mixing techniques either Lagrange multipliers are required.

Of particular importance was the problem of the eight layer composite beam discussed in Section 5.1. For this case, Fig. 31 shows that the error distribution is not monotonous. It means that with a heavier model, one can obtain a higher error than with a lighter one. In other words, the distribution and optimization of the Lagrange points patterm over the thickness, is a key step in the modeling process.

For the case of the eigth-layer beam structure with, Fig. 23 shows the trends of accuracy for both displacement and stresses, with respect to the analytical results. Clearly, the error distribution is not monotonous. It means that with a heavier model, one can obtain a higher error than with a lighter one. In other words, the distribution and optimization of the

Lagrange points patterm over the thickness (namely, the ESL model), is a key step in the modeling process.

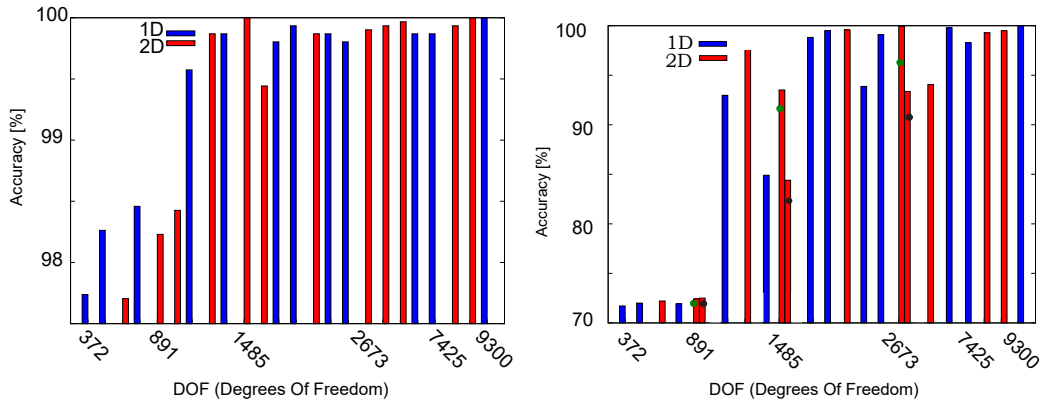

(a) (b)

Figure 23: Transverse displacement and shear stress percentage accuracy with respect to the reference analytical solution ([55]) of the eigth-layer beam case.

References

[1] E. Carrera. Historical review of zig-zag theories for multilayered plates and shells. *Applied Mechanics Reviews*, 56(3):287–308, 2003.

[2] R.K. Kapania and S. Raciti. Recent advances in analysis of laminated beams and plates. Part I: Shear effects and buckling. *AIAA Journal*, 27(7):923–935, 1989.

[3] R.K. Kapania and S. Raciti. Recent advances in analysis of laminated beams and plates. Part II: Vibrations and wave propagation. *AIAA Journal*, 27(7):935–946, 1989.

[4] J.N. Reddy and D.H. Robbins Jr. Theories and computational models for composite laminates. *Applied Mechanics Reviews*, 47(6):147–169, 1994.

[5] T.K. Varadan and K. Bhaskar. Review of different laminate theories for the analysis of composites. *Journal-Aeronautical Society of India*, 49:202–208, 1997.

[6] E. Carrera. Developments, ideas, and evaluations based upon reissner's mixed variational theorem in the modeling of multilayered plates and shells. *Applied Mechanics Reviews*, 54(4):301–329, 2001.

[7] L. Euler. *Methodus inveniendi lineas curvas maximi minimive proprietate gaudentes sive solutio problematis isoperimetrici latissimo sensu accepti*, volume 1. Springer Science & Business Media, Berlin, Germany, 1952.

[8] S.P. Timoshenko. On the transverse vibrations of bars of uniform cross section. *Philosophical Magazine*, 43:125–131, 1922.

[9] N.G. Stephen and M. Levinson. A second order beam theory. *Journal of Sound and Vibration*, 67(3):293–305, 1979.

[10] V. Z. Vlasov. *Thin-walled elastic beams*. National Technical Information Service, Springfield, Virginia, USA, 1984.

[11] R. D. Ambrosini, J. D. Riera, and R. F. Danesi. A modified vlasov theory for dynamic analysis of thin-walled and variable open section beams. *Engineering Structures*, 22(8):890–900, 2000.

[12] I. Mechab, N. El Meiche, and F. Bernard. Analytical study for the development of a new warping function for high order beam theory. *Composites Part B: Engineering*, 119:18–31, 2017.

[13] P.O. Friberg. Beam element matrices derived from vlasov's theory of open thin-walled elastic beams. *International Journal for Numerical Methods in Engineering*, 21(7):1205–1228, 1985.

[14] N.-I. Kim and J. Lee. Exact solutions for coupled responses of thin-walled fg sandwich beams with non-symmetric cross-sections. *Composites Part B: Engineering*, 122:121–135, 2017.

[15] R. Schardt. Eeine erweiterung der technischen biegetheorie zur berechnung prismatischer faltwerke. *Der Stahlbau*, 35:161–171, 1966.

[16] N. Peres, R. Gonçalves, and D. Camotim. First-order generalised beam theory for curved thin-walled members with circular axis. *Thin-Walled Structures*, 107:345–361, 2016.

[17] N. Silvestre. Generalised beam theory to analyse the buckling behaviour of circular cylindrical shells and tubes. *Thin-Walled Structures*, 45(2):185–198, 2007.

[18] N. Silvestre and D. Camotim. First-order generalised beam theory for arbitrary orthotropic materials. *Thin-Walled Structures*, 40(9):755–789, 2002.

[19] N. Silvestre and D. Camotim. Second-order generalised beam theory for arbitrary orthotropic materials. *Thin-Walled Structures*, 40(9):791–820, 2002.

[20] G. Kirchhoff. Über das gleichgewicht und die bewegung einer elastischen scheibe. *Journal für die reine und angewandte Mathematik (Crelles Journal)*, 1850(40):51–88, 1850.

[21] A.E.H. Love. *A treatise on the mathematical theory of elasticity*. Cambridge University Press, Cambridge, UK, 1927.

[22] E. Reissner and Y. Stavsky. Bending and stretching of certain types of heterogeneous aeolotropic elastic plates. *Journal of Applied Mechanics*, 28:402–408, 1961.

[23] E. Reissner. The effect of transverse shear deformation on the bending of elastic plates. *Journal of Applied Mechanics*, 12:69–77, 1945.

[24] R. Mindlin. Influence of rotary inertia and shear flexural motion of isotropic, elastic plates. *Journal of Applied Mechanics*, 18:31–38, 1951.

[25] C.W. Pryor Jr and R.M. Barker. A finite-element analysis including transverse shear effects for applications to laminated plates. *AIAA Journal*, 9(5):912–917, 1971.

[26] A.K. Noor and M.D. Mathers. Finite element analysis of anisotropic plates. *International Journal for Numerical Methods in Engineering*, 11(2):289–307, 1977.

[27] T.J.R. Hughes and T. Tezduyar. Finite elements based upon mindlin plate theory with particular reference to the four-node bilinear isoparametric element. *Journal of Applied Mechanics*, 48:587–596, 1981.

[28] J.N. Reddy. A simple higher-order theory for laminated composite plates. *Journal of Applied Mechanics*, 51:745–752, 1984.

[29] E. Carrera. Evaluation of layerwise mixed theories for laminated plates analysis. *AIAA Journal*, 36(5):830–839, 1998.

[30] T. Kant, D.R.J. Owen, and O.C. Zienkiewicz. A refined higher-order C° plate bending element. *Computers & Structures*, 15(2):177–183, 1982.

[31] T. Kant and J.R. Kommineni. Large amplitude free vibration analysis of cross-ply composite and sandwich laminates with a refined theory and C° finite elements. *Computers & Structures*, 50(1):123–134, 1994.

[32] J.N. Reddy. *Mechanics of laminated composite plates and shells: theory and analysis*. CRC press, New York, USA, 1997.

[33] A.N. Palazotto. *Nonlinear analysis of shell structures*. AIAA Education Series, Reston, Virginia, USA, 1992.

[34] H. Murakami. Laminated composite plate theory with improved in-plane responses. *Journal of Applied Mechanics*, 53:661–666, 1986.

[35] V.R. Aitharaju. C° zigzag kinematic displacement models for the analysis of laminated composites. *Mechanics of Composite Materials and Structures*, 6(1):31–56, 1999.

[36] Y.B. Cho and R.C. Averill. First-order zig-zag sublaminate plate theory and finite element model for laminated composite and sandwich panels. *Composite Structures*, 50(1):1–15, 2000.

[37] F.G. Rammerstorfer, K. Dorninger, and A. Starlinger. Composite and sandwich shells. In *Nonlinear Analysis of Shells by Finite Elements*, pages 131–194. Springer, 1992.

[38] J.N. Reddy. An evaluation of equivalent-single-layer and layerwise theories of composite laminates. *Composite Structures*, 25(1-4):21–35, 1993.

[39] A.S. Mawenya and J.D. Davies. Finite element bending analysis of multilayer plates. *International Journal for Numerical Methods in Engineering*, 8(2):215–225, 1974.

[40] A.K. Noor and W.S. Burton. Assessment of computational models for multilayered composite shells. *Applied Mechanics Reviews*, 43:67–97, 1990.

[41] A.S.D. Wang and F.W. Crossman. Calculation of edge stresses in multi-layer laminates by sub-structuring. *Journal of Composite Materials*, 12(1):76–83, 1978.

[42] N.J. Pagano and S.R. Soni. Global-local laminate variational model. *International Journal of Solids and Structures*, 19(3):207–228, 1983.

[43] R. Jones, R. Callinan, K.K. Teh, and K.C. Brown. Analysis of multi-layer laminates using three-dimensional super-elements. *International Journal for Numerical Methods in Engineering*, 20(3):583–587, 1984.

[44] M.B. Dehkordi, M. Cinefra, S.M.R. Khalili, and E. Carrera. Mixed LW/ESL models for the analysis of sandwich plates with composite faces. *Composite Structures*, 98:330–339, 2013.

[45] M.B. Dehkordi, S.M.R. Khalili, and E. Carrera. Non-linear transient dynamic analysis of sandwich plate with composite face-sheets embedded with shape memory alloy wires and flexible core-based on the mixed LW (layer-wise)/ESL (equivalent single layer) models. *Composites Part B: Engineering*, 87:59–74, 2016.

[46] L. Dozio and E. Carrera. A variable kinematic ritz formulation for vibration study of quadrilateral plates with arbitrary thickness. *Journal of Sound and Vibration*, 330(18-19):4611–4632, 2011.

[47] M. D'ottavio and E. Carrera. Variable-kinematics approach for linearized buckling analysis of laminated plates and shells. *AIAA Journal*, 48(9):1987–1996, 2010.

[48] E. Carrera, A. Pagani, and S. Valvano. Shell elements with through-the-thickness variable kinematics for the analysis of laminated composite and sandwich structures. *Composites Part B: Engineering*, 111:294–314, 2017.

[49] E. Carrera. Theories and finite elements for multilayered, anisotropic, composite plates and shells. *Archives of Computational Methods in Engineering*, 9(2):87–140, 2002.

[50] E. Carrera. Theories and finite elements for multilayered plates and shells: a unified compact formulation with numerical assessment and benchmarking. *Archives of Computational Methods in Engineering*, 10(3):215–296, 2003.

[51] K. J. Bathe. *Finite Element Procedure*. Prentice hall, Upper Saddle River, New Jersey, USA, 1996.

[52] T.J.R. Hughes. *The Finite Element Method: Linear Static and Dynamic Finite Element Analysis*. Courier Corporation, Chelmsford, Massachusetts, USA, 2012.

[53] E. Carrera, M. Cinefra, M. Petrolo, and E. Zappino. *Finite element analysis of structures through unified formulation*. John Wiley & Sons, Hoboken, USA, 2014.

[54] E. Carrera, G. Giunta, and M. Petrolo. *Beam structures: classical and advanced theories*. John Wiley & Sons, Hoboken, USA, 2011.

[55] K.S. Surana and S.H. Nguyen. Two-dimensional curved beam element with higher-order hierarchical transverse approximation for laminated composites. *Computers & Structures*, 36(3):499–511, 1990.

[56] E. Carrera and A. Ciuffreda. A unified formulation to assess theories of multilayered plates for various bending problems. *Composite Structures*, 69(3):271–293, 2005.

[57] N.J. Pagano and S.J. Hatfield. Elastic behavior of multilayered bidirectional composites. *AIAA Journal*, 10(7):931–933, 1972.

[58] J.G. Ren. Exact solutions for laminated cylindrical shells in cylindrical bending. *Composites Science and Technology*, 29(3):169–187, 1987.